Applied Physics B (2018) 124:205
https://doi.org/10.1007/s00340-018-7074-y

Applied Physics B
Lasers and Optics

Nonlinear optical studies of sodium borate glasses embedded with gold nanoparticles

Jagannath Gangareddy[1] · Eraiah Bheemaiah[1] · Vinitha Gandhiraj[2] · Jaimson T. James[3] · Jephin K. Jose[3] · Krishnakanth Katturi Naga[4] · Venugopal Rao Soma[4]

Received: 26 May 2018 / Accepted: 23 September 2018

Abstract
Optical glasses possessing large third-order optical nonlinear susceptibility and fast response times are promising materials for the development of advanced nonlinear photonic devices. In this context, gold nanoparticle (NP)-doped borate glasses were synthesized via the melt-quench method. The nonlinear optical (NLO) properties of thus prepared glasses were investigated at different wavelengths (i.e., at 532 nm using nanosecond pulses, at 750 nm, 800 nm, and 850 nm wavelengths using femtosecond, MHz pulses). At 532 nm, open aperture (OA) Z-scan signatures of gold NP-doped borate glasses demonstrated reverse saturable absorption (RSA), attributed to mixed intra-band and interband transitions, while in the 750−850 nm region, the OA Z-scan data revealed the presence of saturable absorption (SA), possibly due to intra-band transitions. The NLO coefficients were evaluated at all the spectral regions and further compared with some of the recently reported glasses. The magnitudes of obtained NLO coefficients clearly demonstrate that the investigated glasses are potential materials for photonic device applications.

1 Introduction

In the recent past, significant progress has been made in the synthesis, design, and application of bulk materials comprising metal nanostructures [1] because of their fascinating attributes such as superior magnetic, nonlinear optical (NLO), thermal, luminescence, and electrical properties etc. [2, 3]. The properties of noble metal nanoparticles (MNPs, such as Cu, Ag, and Au) have been studied extensively in the past decades by several researchers. Among all noble MNPs, gold nanoparticles (NPs) have been paid a special attention because of their ever growing and fascinating applications in various fields like sensors, biological labelling and detection, solar cell, catalysis, optical limiting, optical switching, and electronics [4] and the toxicity of Au is less compared to other noble metals which is essential for biological applications [5] and also gold NPs possess superior physical properties [6]. Among several applications in the above-said areas, the use of MNPs in the NLO area triggers great interest, since plasmonic optical properties of gold NPs due to electromagnetic field induced collective oscillations of surface plasmons [7] yields good nonlinear coefficients at surface plasmon resonance (SPR) region and even at off SPR regions which is essential for nonlinear device fabrications. There are different transparent media (typically, polymers, liquids, and glasses) for MNPs dispersion which can trigger the optical nonlinearity for about several orders of magnitude, but transparent glass matrices exceptionally attractive, because, as compared to other media, the glass medium has greater advantages such as high mechanical and chemical robustness, high transparency, homogeneous dispersion of MNP, high attenuation coefficient due to light scattering, biocompatibility and the ease of fabrication in desired shapes which also includes planar waveguides and fibers [8, 9] and also the glasses can produced in a larger volume at low cost [10]. Nonetheless, in recent past, there have been several studies on the NLO investigations in vitreous materials in view of

✉ Eraiah Bheemaiah
eraiah@rediffmail.com

Venugopal Rao Soma
soma_venu@uohyd.ac.in

[1] Department of Physics, Bangalore University, Bengaluru, Karnataka 560056, India

[2] Division of Physics, School of Advanced Sciences, VIT Chennai, Chennai, Tamilnadu 600127, India

[3] Department of Physics, Christ University, Bengaluru, Karnataka 560029, India

[4] Advanced Centre of Research in High Energy Materials (ACRHEM), University of Hyderabad, Hyderabad 500046, India

Published online: 01 October 2018

improving the nonlinear optical coefficients in the glasses; for improving the NLO coefficient in the glasses, the one way is to choose the heavy metal oxide or oxides (HMO or HMOs) in the glass composition (since HMOs possess larger electronic polarizability). However, the alternative idea is the doping of MNPs into the glasses, since the distinctive feature of MNPs, i.e., SPR can yield improvement in NLO susceptibility to still larger values at SPR region and at near SPR region due to local electric field effect [7]. In the literature, there are numerous reports on NLO properties of a variety of glasses such as phosphate, tellurite, germanate, and silicate glasses [11, 14−14] and these studies proved that germanate and silicate glasses possess strong nonlinearity. However, the melting temperature and operating temperature of those silicate and germanate glasses are high, and therefore, it is imperative to search new class of glass formers, wherein these hurdles can be circumvented and possess high nonlinearity. In view of these properties, borate-based glasses are widespread in the current use because of their well-known capability of metal ion dispersal, low working and melting temperatures, low temperature of glass transition (T_g), excellent thermal stability, high infrared transmission, and high thermal expansion coefficient (which allows the ease of optical fiber preparation) [9, 11]. For synthesising the MNP inside the glass matrices, there are a number of methods reported in the literature. Using a chemical reduction technique, MNPs have been prepared on the glass slide [15], Qiu et al. [16] recently demonstrated the photo-reduction of Ag atoms from Ag^+ ions in silicate glasses by focusing femtosecond (fs) laser pulses, Yoshio et al. [17] have reported the preparation of gold NPs inside the silica matrices via the sol–gel technique, and Mohr et al. [18] have explained the manipulation of Ag-NPs using ion exchange with post-heat treatment in a reducing atmosphere. However, the above-said techniques along with others such as physical vapour deposition (PVD) and chemical vapour deposition (CVD) methods are expensive and require extensive experimental facilities. Therefore, the melt-quench technique is the convenient, rapid, cost effective and it is not requires a specialized laboratory facility except furnace with dust-free lab, and also in this technique, the NPs distribution is uniform. However, the direct production of MNPs inside the glasses in melt-quench approach is an arduous task due to oxidation processes occurring at elevated temperature while melting the precursors. Douglas et al. [19] have recently demonstrated that choosing the thermal reducing agent in the glass composition produces a highly uniform and homogeneous distribution of MNPs inside the glasses. In addition to the considerable reports on NLO properties glasses doped with MNPs, recently, Rajaramakrishna et al. [20] have reported that gold NP-doped borate glasses demonstrated good saturable absorption (SA) at 532 nm, nanosecond (ns) pulses. Zhong et al. [21] reported reverse saturable absorption (RSA) in copper NP-doped sodium borosilicate glasses at 800 nm with fs-pulse excitation. Furthermore, by studying the temporal dynamics of HMO glasses embedded with Au-NPs using Kerr gate measurements at 780 nm using 120 fs pulses, Almedia et al. [22] have found that the response time was 220 fs (which was faster than the pulse duration). However, there are very few reports on the comparison of NLO properties using different wavelengths in glasses. Furthermore, in our previous work [5], we demonstrated that the gold-doped glasses possessed good SA when excited at 800 nm due to intra-band transitions within the Au-NPs. However, for developing the materials (here the case of glasses) for practical applications in nonlinear optics and photonics, it is also important to study the properties at different wavelengths, since the nonlinearities in glasses (or in any material) are due to different physical mechanisms and those nonlinearities are dependent on pump wavelength, laser pulse widths and peak intensities of laser pulses. Quantifying the optical nonlinearities with different excitation wavelengths and laser pulse durations yields useful information regarding the mechanism involved in the observed nonlinearities and in identification of possible applications of their nonlinearities. For example, optical limiting applications, in general, require the information on nonlinear absorption from studies using ns pulses, while the optical switching applications demand the knowledge of the magnitude and response time of the nonlinear refractive index (n_2) using fs pulses. Furthermore, NLO studies with fs pulses provide information about the multi-photon absorption or SA capabilities which find applications in mode-locking. Similar arguments can be extended for wavelength-dependent studies also. It is imperative to identify the strengths of each new material prepared by performing extensive studies. There are cases, where materials find strong NLO coefficients in the visible spectral region, whereas in certain cases, they could be good in the near-infrared spectral region. Wavelength-dependent studies will provide necessary evidence about the resonance effects. Therefore, in the present communication, we report the NLO properties of gold NPs embedded antimony sodium borate glasses at visible region (532 nm, ns excitation) and at near infra-red (IR) region (750 nm, 800 nm, and 850 nm, fs excitation) and discuss possible mechanisms responsible for the observed optical nonlinearities. Furthermore, the obtained NLO coefficients are compared with some recently reported materials of interest.

2 Experiments and characterization

The detailed procedure for preparation of Au-NPs via melt-quenching technique in borate glasses with wide composition range of $2Sb_2O_3-25Na_2O-73B_2O_3-xAuCl_3$ ($x=0.005$, 0.01 and 0.02 mol%, here after coded as NB-1, NB-2 and NB-3, respectively) has been explained in our previous report [5]. The glass samples approximately having a thickness of 1 mm were used for UV−visible (UV−Vis)

and Z-scan characterizations, whereas for high-resolution transmission electron microscope (HR-TEM) measurements, the fine powder was used. Using Perkin Elmer Lambda-35 UV−Vis spectrometer, the room temperature (RT) UV−Vis absorption spectra were collected in the wavelength range of 200–1100 nm with a spectral resolution of ± 1 nm. The existence, shape, and size of metallic gold NPs in the prepared glass sample were disclosed using HR-TEM (Technica G2, F30) measurements operating at accelerating potential of 300 kV having a resolution of 2 Å. Nonlinear measurements (absorption and refraction) of highly optical bulk glass samples were measured using Z-scan technique [23]. The NLO measurements were performed at different spectral regions (i.e., at 532 nm and ns pulses, at 750 nm, 800 nm, and 850 nm using fs pulses). In the case of 532 nm excitation, 5 ns laser pulses at a repetition rate of 1 Hz from a frequency-doubled Nd:YAG laser (Quanta Ray, M/s Spectra Physics) were utilized. In the case of near-IR excitation, 150 fs (80 MHz) pulses from Ti:sapphire laser (Chameleon, M/s Coherent Inc. operating in the spectral range of 670−1040 nm) were used. In Z-scan experiments, a lens was used for focusing the laser beam and optically polished sample was moved along the *Z*-axis (beam axis) through the focal region over several times that of the diffraction length. At each Z (i.e., position of the sample), the sample experiences a different intensity of the laser beam, and at each position, the transmitted energy was measured with the help of energy meter placed after the sample.

3 Results and discussion

The as-synthesized glass samples were ruby in colour (while undoped glasses were transparent and not discussed here), the change of such colour was analysed by linear absorption spectrum and is displayed in Fig. 1. The samples present a broad SPR absorption band centred at 565 nm, and this occurrence of SPR peak is attributed to the band-to-band transition in Au-NPs (i.e., from the 'd' band to the s−p conduction band of the Au-NPs) [24]. From Fig. 1, it is evident that the SPR-resonant absorption peak of Au-NPs is shifted towards higher wavelength (or lower energy) side from 565 to 597 nm when the doping concentration of gold increased from 0.005 to 0.02 mol% (SPR peak for NB-1 is at 565 nm, for NB-2 the peak is at 590 nm and for NB-3 the peak is at 597 nm). In general, the location of the SPR of the MNP is sensitive to the size, shape, inter-particles distance, and concentration of the MNPs along with the refractive index of dielectric medium [25, 27−27]. It is well understood that, with increase in doping concentration of gold, the density of Au-NPs or gold atomic concentration is increases which in turn responsible for the refractive index increment [5, 26] and the growth of size of the Au-NPs occurs due to Ostwald

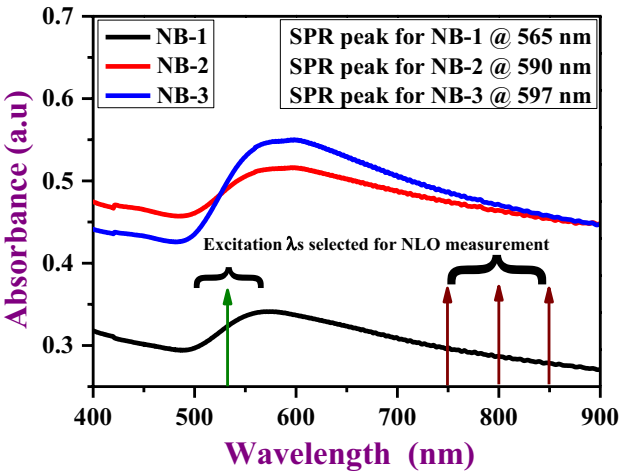

Fig. 1 UV−visible absorption spectra of gold-doped glasses, vertical arrows inside the figure represent the wavelengths chosen for NLO measurements

ripening process [27]. Therefore, the observed red-shift of SPR absorption peak of Au-NPs with enhancement in gold content is due to (i) increase of Au-NP density and (ii) growth of Au-NP size. The same kind of observation (i.e., red-shift of SPR-resonant absorption peak of Au-NPs) is also made by Ju et al. [26] due to increase in refractive index of surrounding medium and by Ghoshal et al. [27] due to size growth of Au-NPs following Ostwald ripening process.

Theoretically, the particle size of MNPs embedded in glasses can be calculated by applying Mie applying theory [28]. The size of the particle is given by [29]

$$R = V_{\mathrm{f}} \frac{\hbar}{\Delta E} \tag{1}$$

$$d = 2R = 2\frac{\hbar V_{\mathrm{f}}}{\Delta E}, \tag{2}$$

where '$\hbar$' is the Plank's constant, 'd' is the average particle diameter of the Au-NPs, 'V_{f}' be the Fermi velocity of bulk gold (13.82×10^5 ms^{-1}) [30], and 'ΔE' is the energy spread and has been calculated from the full width at half maximum (FWHM) of the optical absorption band. Equation (2) is valid only for spherical shaped NPs and also the size of the NPs should be smaller than mean free path of the electrons in bulk metal (for gold the mean free path is 37.7 nm) [30]. The average particle sizes of Au-NPs embedded in the present glasses estimated using Eq. (2) are 20.01, 25.76, and 29.57 nm for NB-1, NB-2, and NB-3, respectively.

HR-TEM is the best technique to characterize the sizes and shapes of the MNPs in various matrices. In the present investigation, the HR-TEM measurements were carried out for NB-1 and NB-2 glasses. HR-TEM micrographs and corresponding histograms are shown in Fig. 2. Figure 2a

illustrates homogenous and closely spaced Au^0 NPs in NB-1 glass, and Fig. 2b represents the corresponding histogram of Au-NPs, says that the size of the Au-NPs in NB-1 glass is in the range of 8−30 nm with an average particle size of 19 nm. Figure 2c represents the homogenous and closely spaced Au^0 NPs in NB-2 glass, and Fig. 2d represents the corresponding histogram of Au-NPs and tells that the size of the Au-NPs in NB-2 glass is in the range of 8−45 nm with an average particle size of 25 nm. Most of the Au-NPs in NB-1 and NB-2 glasses are spherical in nature. The size distribution of the NPs is estimated using the ImageJ software. Insets of Fig. 2a, c represent the selected area electron diffraction (SAED) of Au-NPs in NB-1 and NB-2 glasses, which signifies the presence of (1 1 1) and (2 2 0) planes of Au^0 NPs and are assigned using JCPDS card no. 4−784.

Au atomic concentration (N) and Au−Au interparticle spacing (d_{Au-Au}) were calculated using the relation mentioned in the ref [5]. The Au atomic concentration, Au−Au interparticle spacing, and the Au-NP sizes (estimated using both TEM images and from Mie theory) are tabulated in Table 1. From the data presented in Table 1, it is evident that the average particle size of Au-NPs in NB-1 and NB-2 glasses estimated using Eq. (2) matched well with those evaluated from the TEM images. In addition, it also evident that the particle size increased with the doping concentration of Au. Therefore, from Table 1, it is very clear that the red-shift of SPR peak of Au-NPs is attributed to the size growth of Au-NPs and increase in density of the Au-NPs occurred with respect to the doping concentration of Au. Furthermore, red-shift and broadening of the SPR peak of gold NPs are also due to decrease in Au–Au interparticle distance (d_{Au-Au}) with increase in mol% of the Au [27].

In the present glass system, Sb_2O_3 was used to reduce Au^{3+} to Au^0, and this reduction of $Au^{3+} \rightarrow Au^0$ can be explained by considering reduction potentials (E^0) of the corresponding redox components present in the glass matrix [31]. In glass melts, the E^0 values of multivalent elements may be different compared to those in solutions and are varied with temperature (i.e., temperature dependent). In addition, because of the unavailability of values of E^0 in

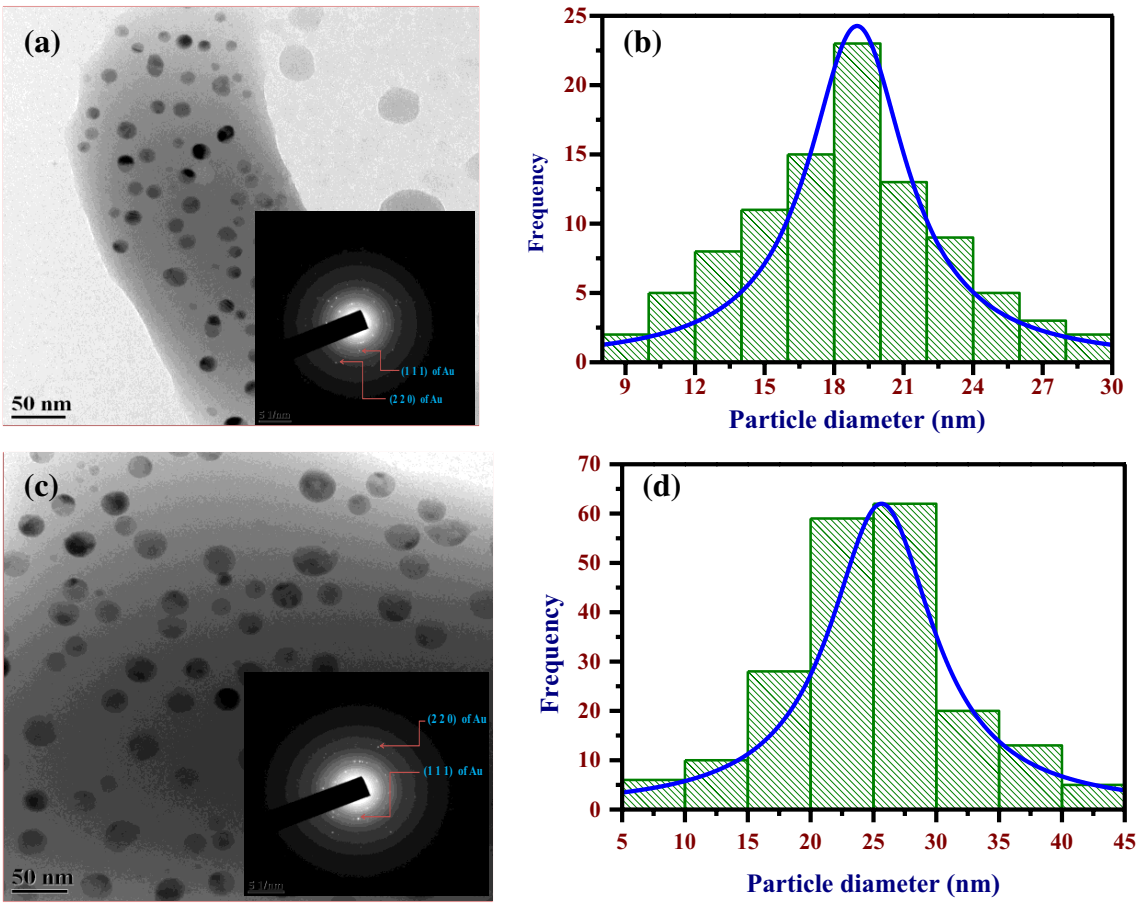

Fig. 2 **a** HR-TEM image depicting uniformly distributed spherical gold NPs in NB-1 glass, **b** corresponding histogram of Au-NPs in NB-1 glass, **c** HR-TEM photograph representing closely distributed spherical gold NPs in NB-2 glass, **d** corresponding histogram of Au-NPs in NB-2 glass. Insets of **a** and **c** are the SAED pattern of the Au-NPs in NB-1 and NB-2 glasses, respectively

Table 1 Variation of the plasmonic properties of Au-NPs in NB glasses: Au-NP size (d), Au atomic concentration (N), and Au−Au interparticle spacing (d_{Au-Au})

Glass samples	N ($\times 10^{20}$ atoms/cm^3)	d_{Au-Au} (nm)	d (from Mie theory) (nm)	d (from TEM images) (nm)
NB-1	1.04	2.16	20.01	19
NB-2	2.06	1.72	25.76	25
NB-3	4.03	1.38	29.57	–

the literature for Sb_2O_3 in glasses at elevated temperature, the room temperature (RT) E^0 values for simple systems at equilibrium with air are used here:

$$Sb^{5+}/Sb^{3+},\ E^0 = 0.649\ \text{V} \tag{3}$$

$$Au^{3+}/Au^0,\ E^0 = 1.498\ \text{V}. \tag{4}$$

In above, the exclusive probable reduction reaction (spontaneous) is $3Sb^{3+}+2Au^{3+}\rightarrow 3Sb^{5+}+2Au^0$ for which E^0 is 1.05 V and free energy (ΔG) is −608 kJ. Thus, free energy with negative sign of the reduction reaction clearly demonstrates that the reaction is thermodynamically feasible and spontaneous, i.e., Sb^{3+} reduces Au^{3+}–Au^0 and Sb^{3+} is self-oxidized to Sb^{5+}.

The NLO absorption and refraction measurements were carried out using OA and CA modes of Z-scan techniques, respectively. In Z-scan measurements the peak intensities (I_{00}) were in the range of 4×10^7–5×10^7 Wcm^{-2} for 532 nm excitation and 5×10^8–8×10^8 Wcm^{-2} for near-IR excitations. In the measurement of NLO properties in Z-scan experiment, the position of the sample versus transmission curve can be plotted by noting the transmitted energy at various positions of the samples using a detector. Figure 3a, b illustrates the recorded OA and CA Z-scan data of the gold-doped glass samples, respectively, at 532 nm, in which the experimental data are represented by open circles and theoretical fits to the data points is represented by solid line. The valley at focal point in OA Z-scan signature is the indicative of RSA kind of nonlinearity, whereas the peak followed by a valley in the CA Z-scan represents that n_2 is negative. The optical nonlinear coefficients were evaluated numerically by fitting the experimental Z-scan data using the standard nonlinear optical equations. The same kind of RSA in OA and negative nonlinear refraction in CA Z-scan results were observed by Zhang et al. [32] for CuO quantum dots in Na_2O–CaO–B_2O_3–SiO_2 glasses using Z-scan setup at 1550 nm in which 50 fs pulses at a repetition rate of 50 MHz were used, Rativa et al. [33] in lead germanium oxide amorphous films at 800 nm in which they performed the measurements using Kerr shutter setup utilizing 150 fs pulses at a repetition rate of 76 MHz,

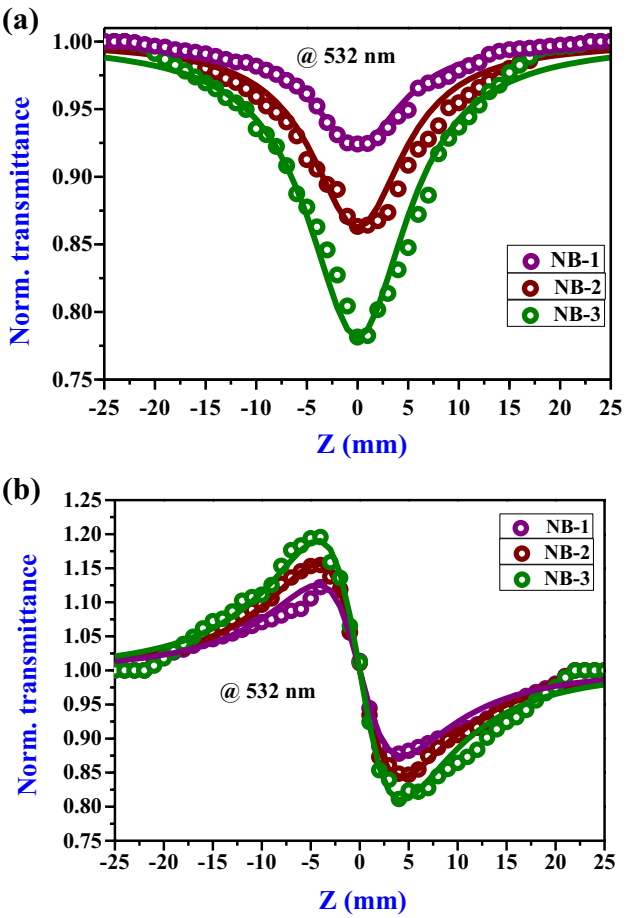

Fig. 3 Z-scan signatures of gold doped NB glasses using ns pulses and 532 nm excitation. **a** OA Z-scan data, **b** CA Z-scan data. Open circles represent the experimental data, while solid lines are theoretical fits

Shanmugavelu et al. [34] in $45Bi_2O_3$−$30ZnO$−$25B_2O_3$ glasses measured with the help of Z-scan technique at 532 nm using 6 ns, 10 Hz pulses, Lin et al. [35] investigated $10Na_2O$−$45B_2O_3$−0.2Al−$50SiO_2$−$4Bi_2O_3$ glasses containing Bi NPs and the measurements were performed using Z-scan method at 800 nm and used 120 fs pulses at a repetition rate of 80 MHz.

We considered the multi-photon absorption (MPA) equation given by Sutherland et al. [36] for computing the nonlinear absorption coefficient:

$$T_{OA}(\text{nPA}) = \frac{1}{\left[1 + (n-1)\,\alpha_n L_{\text{eff}}\left(I_{00}/\left(1 + (Z/Z_0)^2\right)\right)^{n-1}\right]^{1/n-1}}, \tag{5}$$

where α_n is the effective MPA coefficient ($n=2$ for 2PA; $n=3$ for 3PA, and so on) and I_{00} is the peak intensity. For 2PA, ignore all other terms except 2PA term, then the above equation reduces to

$$T_{\mathrm{OA}}(2\mathrm{PA}) = \frac{1}{1 + \alpha_2 L_{\mathrm{eff}}\left(I_{00}/\left(1 + \left(Z/Z_0\right)^2\right)\right)}, \tag{6}$$

where I_{00} is the peak Intensity, Z is the sample position, $Z_0 = \pi\omega_0^2/\lambda$ is the Rayleigh Range, ω_0 is the beam waist at the focal point ($Z=0$), and λ is the laser wavelength, effective path length in the sample of length L, $L_{\mathrm{eff}} = \frac{1-e^{\alpha_0 L}}{\alpha_0}$. The closed aperture Z-scan data were fitted the with following equation [36]:

$$T_{\mathrm{CA}} = 1 + \frac{4\Delta\Phi_0\left(Z/Z_0\right)}{\left[1 + \left(Z/Z_0\right)^2\right]\left[9 + \left(Z/Z_0\right)^2\right]}, \tag{7}$$

where $\Delta\Phi_0$ is the phase difference of the laser beam due to nonlinear refraction and is estimated by fitting the experimental data. In Eq. (7), the sign between two terms is '−ve' for negative nonlinear refraction [37] and is '+ve' for positive nonlinear refraction [34]. The index of nonlinear refraction (n_2) is obtained using

$$n_2\left(\mathrm{m^2\ W^{-1}}\right) = \frac{\left|\Delta\Phi_0\right|\lambda}{2\pi I_{00} L_{eff}}. \tag{8}$$

The measured OA Z-scan data were well fitted with Eq. (6), which concludes that the observed RSA is due to two photon absorption (2PA). The experimental CA Z-scan data also well fitted with Eq. (7). The evaluated values of 2PA and n_2 were tabulated in Table 2.

Figures 4a–c and 5a–c depict the OA and CA Z-scan signatures of gold NP-doped glasses at 750 nm, 800 nm, and 850 nm spectral wavelengths, respectively. The peak at focal point in OA Z-scan represents the SA kind of nonlinearity, whereas the CA Z-scan data are not changed any sign of nonlinear refraction at these wavelengths, which remain as negative nonlinear refraction as that under 532 nm. In Figs. 4 and 5, the open circles representing the experimentally measured data and solid lines are the indicative of theoretically fitted data. The measured nonlinear transmission curves were used to estimate the contributions of SA nonlinearity. Inside the sample, the intensity 'I' varies due to the optical absorption of the sample, according to

$$\frac{\mathrm{d}I}{\mathrm{d}z} = -\alpha\ (I)\ I, \tag{9}$$

where 'Z' is being distance of propagation inside the sample and '$\alpha\ (I)$' is the coefficient of absorption which is dependent with irradiance. When nonlinear processes are absent, then $\alpha\ (I) = \alpha_0$ in the samples, then Eq. (9) is simplified into Beer−Lamberts law of optical absorption [38]. For a better describing of the NLO response, the following absorption coefficient '$\alpha\ (I)$' dependent with intensity is used:

$$\alpha\ (I) = \frac{\alpha_0}{1 + \left(I/I_{\mathrm{S}}\right)} + \beta_{\mathrm{RSA}} I, \tag{10}$$

where 'β_{RSA}' is the nonlinear absorption coefficient (2PA or 3PA or MPA coefficient etc.), 'I' is the intensity of laser beam, and 'I_{S}' is the saturation intensity. In Eq. (10), SA kind of nonlinearity described by first term, while RSA nonlinear property represented by second term. When only RSA kind of nonlinear absorption is present 'I_{S}' will be zero and 'β_{RSA}' will be zero for pure SA. By fitting the OA Z-scan data using Eq. (10) [solid lines in Fig. 4a], the I_{S} values were determined. The same kind of nonlinear results (i.e., SA in OA Z-scan mode and negative nonlinear refraction in CA Z-scan mode) were reported by Chen et al. [39] recently and they reported their investigations on transparent glasses matrix with glass composition of $60Bi_2O_3$–$30B_2O_3$–$10TiO_2$ in which they measured the NLO properties by adopting Z-scan technique at 750 nm using 200 fs laser pulses and a repetition rate of 76 MHz.

The 2PA coefficients (α_2) of Au-NP-doped glasses of present investigation are found to be one order of magnitude greater than that of Na_2O–CaO–B_2O_3–SiO_2 bulk glasses embedded with CuO quantum dots ($\alpha_2 = 1.56 \times 10^{-12}$ m/W at 1550 nm) [32] and that of gold NP-doped heavy metal oxide glasses (α_2 varied from 0.6×10^{-12} m/W to 0.9×10^{-12} m/W for the wavelengths in the range of 500 nm to 580 nm) [22]. The coefficients are comparable to that of sodium borosilicate glasses doped with copper quantum dots ($\alpha_2 = 2.10 \times 10^{-11}$ m/W at 1550 nm) [21] and lower than that of silver-doped oxyfluoride glasses (α_2 ranges from 1.1×10^{-9} m/W to 24.8×10^{-9} m/W at the wavelengths from 445 nm to 660 nm of NPs sizes 3 nm and 17 nm) [39]. Furthermore, the I_{S} values of present glasses are comparable

Table 2 Summary of the NLO coefficients computed for different glasses studied in the present work

Samples	$\lambda = 532$ nm (ns)		$\lambda = 750$ nm (fs)		$\lambda = 800$ nm (fs)		$\lambda = 850$ nm (fs)	
	α_2 (m/W) $\times 10^{-11}$	n_2 (m^2/W) $\times 10^{-16}$	I_s (W/m^2) $\times 10^{10}$	n_2 (m^2/W) $\times 10^{-16}$	I_s (W/m^2) $\times 10^{10}$	n_2 (m^2/W) $\times 10^{-16}$	I_s (W/m^2) $\times 10^{10}$	n_2 (m^2/W) $\times 10^{-16}$
NB-1	1.82 ± 0.18	− 2.84 ± 0.28	7.76 ± 0.77	− 2.79 ± 0.27	7.34 ± 0.73	− 2.71 ± 0.27	7.22 ± 0.72	− 2.62 ± 0.26
NB-2	2.02 ± 0.20	− 3.22 ± 0.32	7.82 ± 0.78	− 3.14 ± 0.31	7.52 ± 0.75	− 3.04 ± 0.30	7.31 ± 0.73	− 2.93 ± 0.29
NB-3	2.41 ± 0.24	− 3.91 ± 0.39	8.00 ± 0.80	− 3.83 ± 0.38	7.81 ± 0.78	− 3.74 ± 0.38	7.62 ± 0.76	− 3.61 ± 0.36

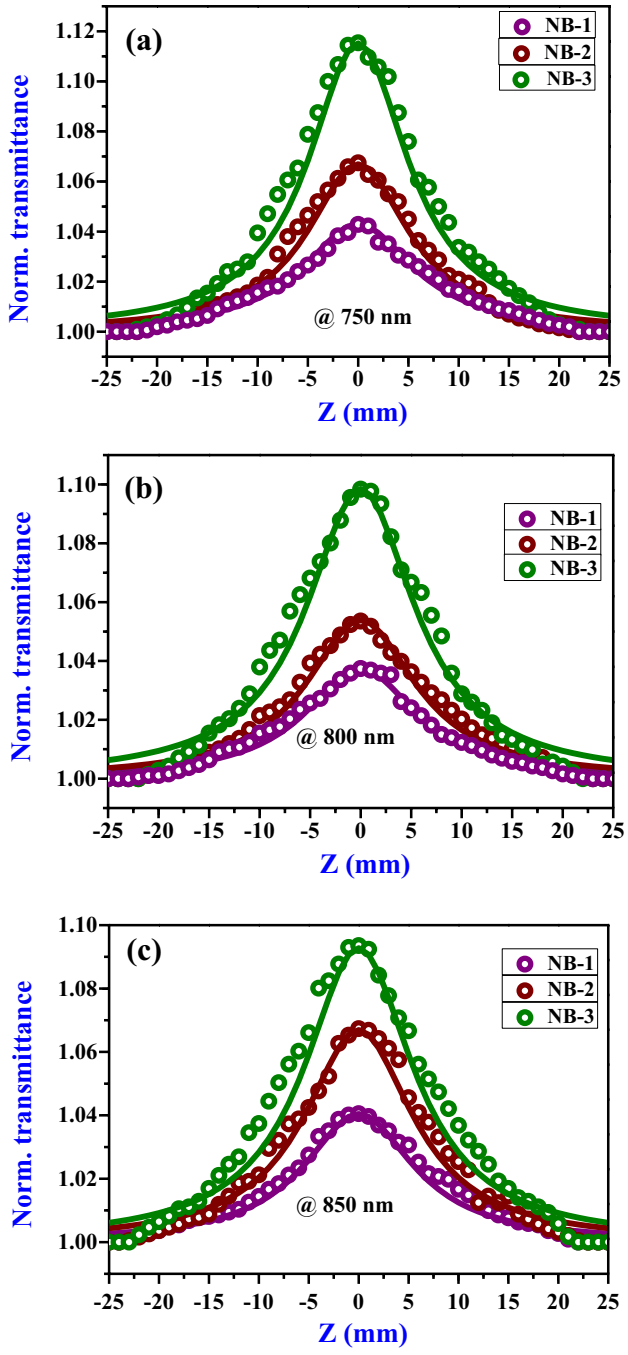

Fig. 4 OA Z-scan plots of NB glasses embedded with gold NPs using fs pulses at different excitation wavelengths of near-IR region **a** at 750 nm, **b** at 800 nm, and **c** at 850 nm. Open circles represent the experimental data, while solid lines are theoretical fits

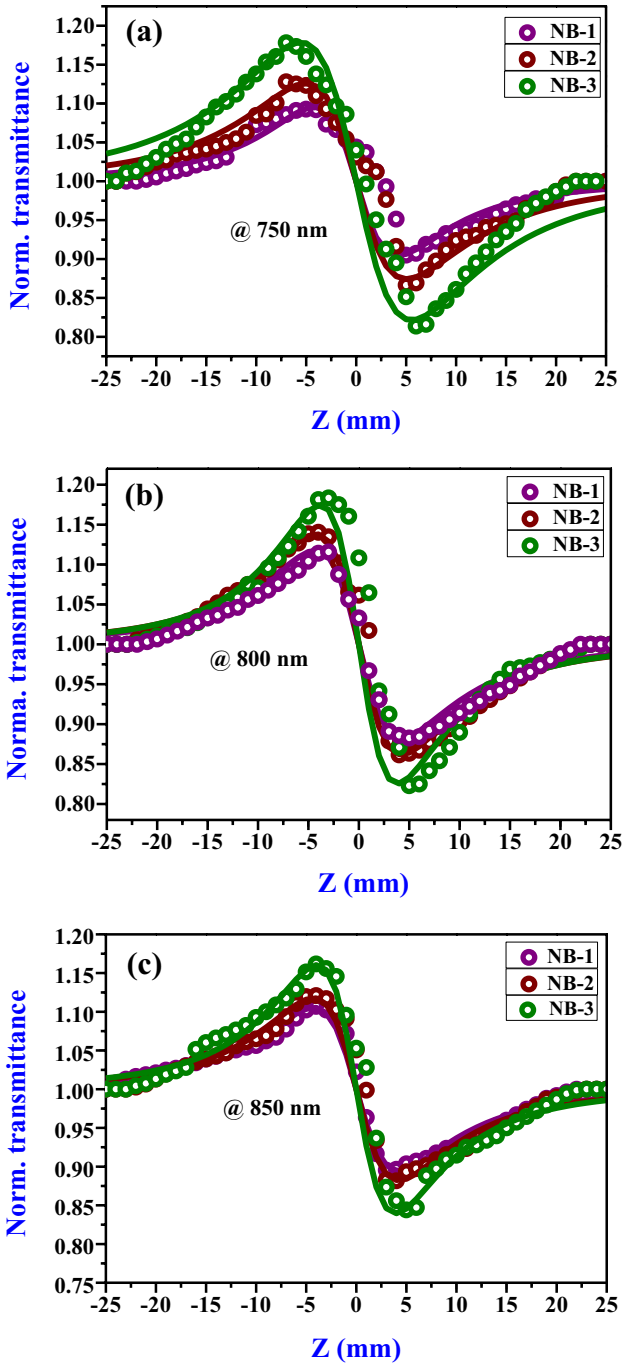

Fig. 5 CA Z-scan plots of NB glasses embedded with gold NPs using fs pulses at different near-IR wavelengths excitations **a** at 750 nm, **b** at 800 nm, and **c** at 850 nm. Open circles represent the experimental data, while solid lines are theoretical fits

with that of silver-doped oxyfluoride glasses (I_S ranged from 5×10^9 W/m^2 to 7×10^{10} W/m^2 at 480 nm for the particle sizes in the range of 2.4 nm and 2.8 nm) [8] and lower than that of silver NPs embedded commercially available BK7 glass ($I_S = 8.5\times10^{15}$ W/m^2 at 800 nm) [40] and also that of Cu^+ implanted fused silica ($I_S = 2.9\times10^{14}$ for 100 keV Cu^+ implanted sample, $I_S = 5\times10^{14}$ for 200 keV Cu^+ implanted sample, the measurements were performed at 532 nm) [41]. Moreover, the n_2 values obtained for present gold NP-doped titled glasses are two order of magnitude greater than that of CuO quantum dots embedded Na_2O–CaO–B_2O_3–SiO_2 bulk glasses ($n_2 = -2.509\times10^{-18}$ m^2/W at 1550 nm) and

lesser than that of $45Bi_2O_3{-}30ZnO{-}25B_2O_3$ glass ($n_2 = -6.9\times10^{-16}$ m^2/W at 532 nm) [34].

Following the arguments provided by Philip et al. [42], in Au-NPs, there are three main transitions, the partial energy-level diagram representing the transitions in Au-NPs is shown in Fig. 6: (i) at 670 nm attributed to 'sp'-to-'sp' band is the first excited transition and is an intra-band transition (sp→sp); (ii) at 450 nm is the combination of 'sp'-to-'sp' band and 'd'-to-'sp' bands; hence, it is an mixed intra-band (sp→sp) and interband (d→sp) transitions; and (iii) at 400 nm is the transition between 'd'-to-'sp' bands (i.e., interband transition from d→sp band), and the corresponding energies of 670 nm, 450 nm, and 400 nm transitions are 1.52 eV, 2.63 eV, and 2.91 eV, respectively. The intra-band transition can be defined as transition of free electrons in valence band to the Fermi surface and this transition is permissible even the excitation radiation has photons of low energy. The transition of electrons from d-band to the conduction band is interband type transition and to induce this type of transition the photons should possess higher energy. In the present NLO studies, Au-NP-doped glasses were excited at 532 nm, and therefore, intra-band and interband transitions are possible, since the energy of laser pulses is considerably high, which generates the free carriers in the conduction band. These newly generated carriers can absorb additional photons from laser pulse by assistance of phonon which results in optical limiting action as seen in OA nonlinear investigation in the present glasses. On the other hand, for the near-IR measurements, the Au-NP-doped bulk glass samples were excited at 750 nm (1.65 eV), 800 nm (1.55 eV), and 850 nm (1.46 eV) and the corresponding energies of excited wavelengths are closer to that of 1.52 eV (670 nm) and smaller than 2.63 eV (450 nm) and 2.91 eV (400 nm). Furthermore, the input peak intensity of laser beam is low enough to induce only SA kind of nonlinearity, which can be attributed to intra-band transition.

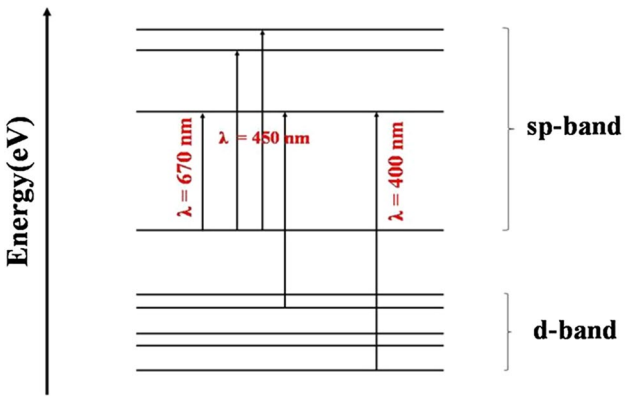

Fig. 6 Typical energy-level diagram representing the three kinds of transitions in Au-NPs

Therefore, it can be concluded that the RSA kind of nonlinearity observed at 532 nm in OA Z-scan data is attributed to the mixed intra-band and interband (sp→sp and d→sp, respectively) transitions, while the SA type of nonlinearity observed in OA Z-scan data at IR spectral excitations is possibly caused due to intra-band (sp→sp) transitions. Recently, Almedia et al. [22] have measured the response time in HMO glasses containing gold NPs through Kerr gate measurements at 780 nm using 120 fs pulses and they found that the response time is 220 fs (faster than the pulse duration). Sugimoto et al. [43] have studied the temporal dynamics of glasses containing Bi_2O_3 through degenerate four wave mixing (DFWM) method at 810 nm using 200 fs laser pulses and found that the studied glasses show electronic response below 200 fs. Similarly, Yu et al. [44] have measured the optical nonlinearity of HMO glasses through the optical Kerr gate method and found that the temporal response was faster than 350 fs. These results show that the obtained nonlinearity originates mostly from electronic processes. The observed negative nonlinear refraction in CA Z-scan mode represents self-defocusing effect. From data summarized in Table 2, it is evident that the α_2, n_2, and I_S values increased with increase in doping content of the gold. This is because with enhancement in concentration of Au doping the density of the NPs' formation increases, which in turn is responsible for the enhanced values. Furthermore, with IR excitation, the trend of I_S and n_2 values is found to increase with wavelength (i.e., coefficients magnitude at 750 nm > 800 nm > 850 nm) and this could be attributed to the SPR peak of Au-NPs (750 nm is closer when compared to 850 nm). Our future work will be focused on extending these studies up to 1.5 μm wavelength region.

4 Conclusions

Antimony sodium borate glasses embedded with gold NPs were synthesized through the method of melt quench. The absorption spectrum evidenced the presence of Au-NPs inside the glass matrix by exhibiting an SPR peak of Au-NPs at 566 nm and is found to red shifted with increase in doping concentration of gold. The HR-TEM images further confirmed the existence of Au^0 NPs having a mean particle size of 19 nm in NB-1 glass and 25 nm in NB-2 glass. OA Z-scan results at 532 nm excitation demonstrated an enhanced RSA due to 2PA which is attributed to mixed intra-band and interband transitions, while in near-IR spectral excitations the glasses demonstrated SA kind of nonlinearity is attributed to intra-band transitions. The OA Z-scan results obtained at 532 nm suggest that the investigated gold NP-doped borate glasses are superior materials for optical limiting applications in visible region (i.e., at 532 nm), while the same glasses are beneficial to mode-locking and nonlinear optical

switching applications for the generation of ultrashort pulses in near-IR region (i.e., from 750 nm to 850 nm).

Acknowledgements One of the authors (GJ) is grateful to Dr. Rajan V Anavekar, former Professor, Department of Physics, Bangalore University, Bangalore, for useful discussions and valuable suggestions. The authors thank Sophisticated Analytical Instrument Facility (SAIF), Indian Institute of Technology, Bombay, India for providing HR-TEM experimental facility. S. V. Rao thanks DRDO, India for financial support through ACRHEM. GJ would like to thank Dr. Promod Kumar, Department of Physics, University of the Free state, Bloemfontein, South Africa for useful inputs given to measure the particle size using Mie theory.

References

1. C. Zheng, J. Huang, L. Lei, W. Chen, H. Wang, W. Li, Appl. Phys. B Lasers Opt. **124**, 17 (2018)
2. H. Fares, H. Elhouichet, B. Gelloz, M. Ferid, J. Appl. Phys. **117**, 1 (2015)
3. H. Jain, A. Issa, R.V. Anavekar, R. Böhmer, O. Kanert, R. Kuchler, Appl. Phys. Lett. **95**, 1 (2009)
4. X. Zhang, W. Luo, L.J. Wang, W. Jiang, J. Mater. Chem. C **2**, 6966 (2014)
5. G. Jagannath, B. Eraiah, K. NagaKrishnakanth, S. Venugopal Rao, J. Non-Cryst. Solids **482**, 160 (2018)
6. C. Feng, M. Liu, Y. Li, X. Gao, Z. Kang, G. Qin, Z. Jia, X. Tao, T. Song, Y. Dun, F. Bai, P. Li, Q. Wang, J. Fang, Appl. Phys. B Lasers Opt. **123**, 81 (2017)
7. Z. Xu, Q. Guo, C. Liu, Z. Ma, X. Liu, J. Qiu, Appl. Phys. B Lasers Opt. **122**, 259 (2016)
8. H.H. Mai, V.E. Kaydashev, V.K. Tikhomirov, E. Janssens, M.V. Shestakov, M. Meledina, S. Turner, G.V. Tendeloo, V.V. Moshchalkov, P. Lievens, J. Phys. Chem. C **118**, 15995 (2014)
9. M.B. Roberge, S.H. Santagneli, S.H. Messaddeq, M. Rioux, Y. Ledemi, H. Eckert, Y. Messaddeq, J. Phys. Chem. C **121**, 13823 (2017)
10. M.M. Hivrekar, D.B. Sable, M.B. Solunke, K.M. Jadhav, J. Non-Cryst. Spldis **474**, 58 (2017)
11. D. Manzani, J.M.P. Almeida, M. Napoli, L.D. Boni, M. Nalin, C.R.M. Afonso, S.J.L. Ribeiro, C.R. Mendonça, Plasmonics **8**, 1667 (2013)
12. T.R. Oliveira, E.L.F. Filho, C.B.D. Araujo, D.S.D. Silva, L.R.P. Kassab, D.M.D. Silva, J. Appl. Phys. **114**, 1 (2013)
13. R.F. Souza, M.A.R.C. Alencar, J.M. Hickmann, R. Kobayashi, L.R.P. Kassab, Appl. Phys. Lett. **89**, 1 (2006)
14. S. Qu, Y. Gao, X. Jiang, H. Zeng, Y. Song, J. Qiu, C. Zhu, K. Hirao, Opt. Commun. **224**, 321 (2003)
15. R. Schneider, R. Schneider, E.A.D. Campos, J.B.S. Mendes, J.F. Felix, P.A.S. Cruz, RSC Adv. **7**, 41479 (2017)
16. J. Qiu, M. Shirai, T. Nakaya, J. Si, X. Jiang, C. Zhu, K. Hirao, Appl. Phys. Lett. **8**, 3040 (2002)
17. Y. Kobayashi, M.A.C. Duarte, L.M.L. Marzan, Langmuir **17**, 6375 (2001)
18. C. Mohr, M. Dubiel, H. Hofmeister, J. Phys. Condens. Matter **13**, 525 (2001)
19. D.F. Franco, A.C. Santana, L.F.C.D. Oliveira, M.A.P. Silva, J. Mater. Chem. C **3**, 3803 (2015)
20. R. Rajaramakrishna, S. Karuthedath, R.V. Anavekar, H. Jain, J. Non–Cryst. Solids **358**, 1667 (2012)
21. J. Zhong, W. Xiang, H. Zhao, W. Zhao, G. Chen, X. Liang, J. Alloys Compd. **537**, 269 (2012)
22. J.M.P. Almeida, D.S. da Silva, L.R.P. Kassab, S.C. Zilio, C.R. Mendonça, L. De Boni, Opt. Mater. **36**, 829 (2014)
23. M.S. Bahae, A.A. Said, T.H. Wei, D.J. Hagan, E.W.V. Stryland, IEEE J. Quantum Electron. **26**, 760 (1990)
24. J. Sasai, K. Hirao, J. Appl. Phys. **89**, 4548 (2001)
25. K.H. Su, Q.H. Wei, X. Zhang, J.J. Mock, D.R. Smith, S. Schultz, Nano Lett. **3**, 1087 (2003)
26. S. Ju, P.R. Watekar, S.G. Kang, J.K. Chung, C.J. Kim, W.T. Han, J. Non-Cryst. Solids **356**, 2578 (2010)
27. S.K. Ghoshal, A. Awang, M.R. Sahar, R. Arifin, J. Lumin. **159**, 265 (2015)
28. G. Mie, Ann. Phys. **330**, 377 (1908)
29. P. Kumar, M.C. Mathpal, A.K. Tripathi, J. Prakash, A. Agarwal, M.M. Ahmad, H.C. Swart, Phys. Chem. Chem. Phys. **17**, 8596 (2015)
30. D. Gall, J. Appl. Phys. **119**, 1 (2016)
31. T. Som, B. Karmakar, J. Opt. Soc. Am. B **26**, 21 (2009)
32. Y. Zhang, J. Zhang, Y. Jin, J. Zhang, G. Hu, S. Lin, R. Yuan, X. Liang, W. Xiang, J. Mater. Sci. Mater. Electron. **28**, 1 (2017)
33. D. Rativa, R.E.D. Araujo, C.B.D. Araujo, A.S.L. Gomes, L.R.P. Kassab, Appl. Phys. Lett. **90**, 1 (2007)
34. B. Shanmugavelu, V.V.R.K. Kumar, R. Kuladeep, D.N. Rao, J. Appl. Phys. **114**, 1 (2013)
35. G. Lin, D. Tan, F. Luo, D. Chen, Q. Zhao, J. Qiu, J. Non–Cryst. Solids **357**, 2312 (2011)
36. R.L. Sutherland, Handbook of nonlinear optics, 2nd edn. (Marcel Dekker, New York, 2003)
37. S.B. Kolavekar, N.H. Ayachit, G. Jagannath, K. NagaKrishnakanth, S. Venugopal Rao, Opt. Mater. **83**, 34 (2018)
38. I. Papagiannouli, P. Aloukos, D. Rioux, M. Meunier, S. Couris, J. Phys. Chem. C **119**, 6861 (2015)
39. F. Chen, T. Xu, S. Dai, Q. Nie, X. Shen, X. Wang, B. Song, J. Non-Cryst. Solids **256**, 2786 (2010)
40. A. Ajami, W. Husinsky, B. Svecova, S. Vytykacova, P. Nekvindova, J. Non-Cryst. Solids **426**, 159 (2015)
41. B. Ghosh, P. Chakraborty, S. Mohapatra, P. Ann Kurian, C. Vijayan, P.C. Deshmukh, P. Mazzoldi, Mater. Lett. **61**, 4512 (2007)
42. R. Philip, P. Chantharasupawong, H. Qian, R. Jin, J. Thomas, Nano Lett. **12**, 4661 (2012)
43. N. Sugimoto, H. Kanbara, S. Fujiwara, K. Tanaka, K. Hirao, Opt. Lett. **21**, 1637 (1996)
44. B.L. Yu, A.B. Bykov, T. Qiu, P.P. Ho, R.R. Alfano, N. Borrelli, Opt.Commun. **215**, 407 (2003)s